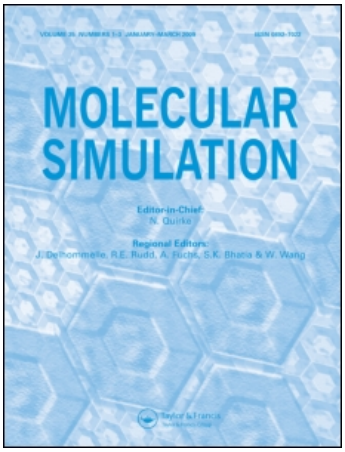

Molecular Simulation
Publication details, including instructions for authors and subscription information:
http://www.informaworld.com/smpp/title~content=t713644482

Microscopic Simulation of Rheology: Molecular Dynamics Computations and Percolation theory

David M. Heyes[a]; John R. Melrose[a]
[a] Department of Chemistry, Royal Holloway and Bedford New College, University of London, Egham, Surrey, UK

To cite this Article Heyes, David M. and Melrose, John R.(1989) 'Microscopic Simulation of Rheology: Molecular Dynamics Computations and Percolation theory', Molecular Simulation, 2: 4, 281 — 300
To link to this Article: DOI: 10.1080/08927028908034606
URL: http://dx.doi.org/10.1080/08927028908034606

Molecular Simulation, 1989, Vol. 2, pp. 281–300
Reprints available directly from the publisher
Photocopying permitted by license only

MICROSCOPIC SIMULATION OF RHEOLOGY: MOLECULAR DYNAMICS COMPUTATIONS AND PERCOLATION THEORY

DAVID M. HEYES and JOHN R. MELROSE

Department of Chemistry, Royal Holloway and Bedford New College, University of London, Egham, Surrey TW20 0EX, UK.

(*Received January 1988*)

The rheology of any liquid can now, in principle, be predicted from first principles using the computer simulation technique of molecular dynamics. Computations on simple molecular fluids close to the solid phase co-existence line have revealed that shear thinning and shear thickening, as well as other non-Newtonian effects are manifest by all liquids at large enough shear rates. This discovery leads to simplifications in predicting non-Newtonian behaviour. The shear viscosity as a function of shear rate for a wide range of disparate experimental and simulated liquids fall on a "universal" curve, when normalised by internally derived parameters.

The rheology of intermediate density fluids at volume fractions *ca.* 25% has not been studied by simulation with the same degree of interpretive success. We reveal that there is a close link between the rheology of this part of the phase diagram and microscopic parameters, using ideas borrowed from *Percolation Theory*. We establish this relationship directly by molecular dynamics simulation. This is a first step towards modelling the rheology of weakly and strongly aggregating colloidal dispersions.

KEY WORDS: Rheology, molecular dynamics, computer simulation, percolation theory, Lennard-Jones potential.

1 INTRODUCTION

1.1 Low and High Density Fluid Rheology

Molecular dynamics simulation has enabled the shear thinning behaviour of model simple molecular fluids (e.g., Ar) to be studied [1–4]. The shear thinning of these fluids occurs at shear rates of order $10^{12}s^{-1}$. This is experimentally inaccessible but is routinely accomplished in a realistic *simulation* of laminar shear flow. This model takes into account the collective motions of the molecules explicitly. Combined with the extensive experimental data on more complicated molecular liquids (e.g., oils [5], colloidal dispersions [6, 7] and sugar/water mixtures [8]), Molecular dynamics has helped show that *all* dense liquids shear thin at a reduced shear rate $\dot{\gamma}\tau \approx 1$ and shear thicken at $\dot{\gamma}\tau \approx 10$–$100$. The latter figure depends somewhat on the acceleration of the viscometer in the experiment, or equivalently the rate of increase of shear rate in the simulation. Figure 1 shows the shear thinning and thickening of a model simple fluid determined by simulation. The shear rate, $\dot{\gamma}$, is made dimensionless by multiplying it by a characteristic time for that material, τ, which is a time for significant local structural change in the unsheared material. For example, for a simple molecule this would be the time it takes a molecule to diffuse a distance comparable to the molecular diameter. For a polymer molecule this time corresponds to some significant stress-relieving segmental motion. This *universal* curve demonstrates that shear thinning and

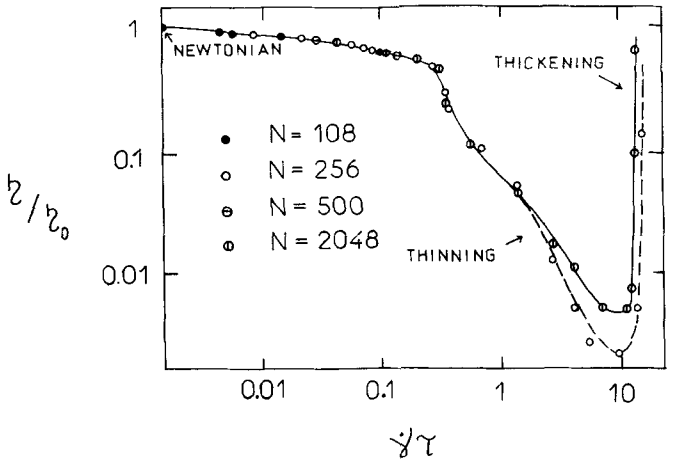

Figure 1 Non-Newtonian rheogram of the *LJ* fluid at $\varrho^* = 0.8442$ and $T^* = 0.722$ by *NEMD* [2]

thickening phenomena have microscopic origins because they are governed by the time for microscopic structural changes. (One could consider the quantity, $\dot{\gamma}^{-1}$, to be a time scale for local structural disruption caused by the imposed shear rate.) For a gas [9] τ is,

$$\tau = 5/\{16\Omega^{22}\varrho\,(\pi k_B T/m)^{1/2}\sigma^2\} \tag{1}$$

where the pair collision integral, $\Omega^{22}(T^*) \approx 1$ For the dense single component fluid [2],

$$\tau = \eta_0/G \tag{2}$$

where η_0 is the viscosity in the limit of zero shear rate and G is the shear modulus. For colloidal dispersions [4],

$$\tau = 3\nu\sigma^3\eta_s/8k_BT \tag{3}$$

where σ is twice the root mean square radius of gyration of the macroparticle and η_s is the viscosity of the suspending fluid.

1.2 Intermediate Density Fluid Rheology

The rheological properties of intermediate density particulate dispersions can change dramatically when they order into clusters of macroscopic dimensions. the shear viscosity, and high frequency shear and compressional moduli of colloidal aggregates, (e.g., sterically stabilised silica particles [6]), microemulsions [10] and macromolecular solutions [11] increase dramatically with volume fraction, ϕ, above a critical value, ϕ_p, associated with the onset of an infinitely spanning cluster. (In two dimensions there is only one infinitely spanning cluster at ϕ_p, and in three dimensions this is also *probably* the case [12].) For particles having a short range attraction (of thickness *Ca.* 0.1 σ beyond the hard core of diameter σ) the value of ϕ_p depends strongly on the ratio of the thermal energy to the depth of the potential well, T^*. Usually ϕ_p changes rapidly in the vicinity of the critical temperature of the system ($T^* \approx 1$), terminating

on the liquid-vapour co-existence curve. Although we will refer to the formation of an infinitely spanning cluster in these molecular fluids as a *Percolation Transition*, this term strictly only refers to a purely geometrical "connectivity" transition [13], without the influence of thermodynamic factors inherent in the experimental systems. At this point it is appropriate to mention that here we are not concerned with the percolation of free volume (as has been considered recently [14]) but of the particulate components, although both uses of the word "percolation" refer to the formation of some kind of unbounded pathway through space. The relationship between these two definitions has not been established, although intuitively a link should exist.

There is a fundamental difference between the origins of non-Newtonian rheology in these intermediate density aggregates and the low and high-density extremes discussed in Section 1.1. At intermediate density, the effect can be attributed to a shear-induced restructuring of tenuous aggregates composed of particles that are in much closer proximity than in a random distribution due to their *attractive* interactions. In contrast, at the low and high density extremes non-Newtonian effects are caused by an interplay between the perturbing shear flow field and the *repulsive* interactions between the particles. At low density this results in a non-Boltzmann distribution of velocities which produces the observed effects, whereas at high density it is mainly configurational in origin. (There is a change in structure of the first co-ordination shell, which results from a competition between the shear perturbation and the small free volume in the fluid.)

To study percolation it is necessary to introduce a parameter, δ. A definition of connectedness of molecules arises via a search diameter $(1 + \delta)\sigma$, where σ is the repulsive core diameter. Two particles are connected if the atomic centres lie within a distance $(1 + \delta)\sigma$ of each other, where periodic boundary conditions are applied to find the nearest image. Of course, the choice of δ should be based on some physical criterion, to be of use in interpreting experimental measurables. This is because we postulate that there is a characteristic distance scale which dominates these physical properties (even for particles interacting via continuous potentials). The value of δ will certainly depend on the physical property of interest. Here we will show that if $(1 + \delta)\sigma$ is just beyond the first peak position in the pair radial distribution function, the percolation transition that results occurs at a density which is pivotal for the density dependence of physical observables, such as pressure, infinite frequency moduli and shear viscosity. In contrast, if one were interested in the transport of excitations between the particles than one would consider $\delta\sigma$ to be a characteristic hopping distance.

Only recently have continuum or "off-lattice" studies of percolation been performed for spherical particles with some form of realistic pair interaction. The square-well fluid of hard core diameter, σ, and pair attraction of depth, $-\varepsilon$, extending to $\sigma(1 + \lambda)$ has been considered with $\lambda = 0.1$ [15] at a range of $T^*(= K_B T/\varepsilon)$. The search diameters for percolation, $\sigma(1 + \delta)$, ranged through the values δ from -0.1 to 1. the infinite temperature limit of this system has also been considered in more detail [16]. Adhesive spheres, which are *not* square-wells in the limit $\lambda \to 0$, have also had their percolation characteristics investigated [17, 18]. The results of these studies can be briefly summarised as follows. We consider first the infinite temperature limit. As δ/σ goes from infinity to zero (the so-called soft-core to hard-core transition) the percolating cluster becomes more tenuous. The most probable number of nearest neighbours at percolation drops from *Ca.* 3 to 1.5 as it becomes less branched (or "ramified") [16]. In these two limits $\phi_p(1 + \delta)^3$ increases because the number of

alternative pathways for percolation diminishes rapidly with $\delta \to 0$ and $\delta \to \infty$. At finite T, ϕ_p drops with increasing δ. In two dimensions for $\delta \gg \lambda$ the quantity ϕ_p can increase as temperature decreases to T_c due to a compaction of the clusters. This is not noticed for $\delta \ll \lambda$. In three dimensions there is no evidence that this occurs.

Despite the obvious intuitively-reasonable link between connectivity and rheology in these systems there has been no attempt, *until this work*, to link rheology and percolation clusters directly from the simulation. (There has been some *analytical* work on the moduli of percolation and higher density clusters in arbitrary dimension [19, 20].) We note also that percolation theory describes the medium only in the vicinity of the percolation transition. Therefore the dense fluid behaviour is outside its realm and the regime of applicability of percolation theory is not known for an arbitrary system.

2 METHOD

2.1 Molecular Dynamics

The simulations were performed on model fluids with N particles in an Molecular dynamics cell of volume V. They interacted through the Lennard-Jones, LJ, potential [2],

$$\phi(r) = 4\varepsilon\{(\sigma/r)^{12} - (\sigma/r)^{6}\} \tag{4}$$

The interactions were truncated beyond a separation r_c equal to 2.5σ. The quantities calculated are expressed in the usual LJ reduced units: distance is in units of σ; energy is in ε; temperature is in ε/k_B; time is in $\sigma(m/\varepsilon)^{1/2}$; pressure and moduli are in ε/σ^3; viscosity is in $(m\varepsilon)^{1/2}/\sigma^2$, the thermal conductivity is in $k_B(m/\varepsilon)^{-1/2}/\sigma^2$ and the self-diffusion coefficient is in $(\varepsilon/m)^{1/2}/\sigma$. We calculated the following properties.

2.1.1 Thermodynamic Quantities

The internal energy, E, has a kinetic and configurational component. Taking pair interactions within a distance r_c, and velocity, v

$$E = \left\langle \frac{0.5}{N} \sum_{i=1}^{N} m_i v_i^2 + \Phi \right\rangle \tag{5}$$

$$\Phi = \left\langle 0.5 \sum_{j=1} \sum_{\substack{i=1 \\ j \neq i}}^{N} \phi_{ij} \right\rangle / N + \Phi_{lrc}$$

The long range correction to the configurational part of Φ is,

$$\Phi_{lrc} = 8\pi\varrho\,((\sigma/r_c)^9/9 - (\sigma/r_c)^3/3) \tag{7}$$

assuming the pair radial distribution function is unity beyond r_c. P is the pressure,

$$P = \left\{ \sum_{i=1}^{N} m_i v^2 - \sum_{i=1}^{N} \sum_{\substack{j=1 \\ i \neq j}}^{N} r_{ij}\,(d\phi_{ij}/dr)/2 \right\} /3V + P_{lrc} \tag{8}$$

Here m_i is the mass of molecule i. If r_i is the position of molecule i then $r_{ij} = r_i - r_j$. The long range correction to the configurational part of the pressure is,

$$P_{lrc} = 16\pi\,\varrho^2\,(2(\sigma/r_c)^9/9 - (\sigma/r_c)^3/3) \tag{9}$$

2.1.2 Mechanical Properties

The infinite frequency shear and bulk moduli are expressible in terms of potential energy components. For the LJ potential we have [21],

$$G_\infty = \varrho k_B T + \varrho(108\Phi_{12} + 18\Phi_6)/15 \tag{10}$$

where Φ_{12} and Φ_6 are the r^{-12} and r^{-6} components of Φ. Similarly [22],

$$K_\infty = 5\varrho k_B T/3 + \varrho(20\Phi_{12} + 6\Phi_6) \tag{11}$$

Note also that by rearrangement we also have [23],

$$G_\infty = 26\varrho k_B T/5 + 3P - 24\varrho E/5 \tag{12}$$

$$K_\infty = 5G_\infty/3 + 2(P - \varrho k_B T) \tag{13}$$

2.1.3 Transport Properties

The self-diffusion coefficient, D, shear viscosity, η, bulk viscosity, η_B, and thermal conductivity, λ, were obtained using the Green-Kubo formulae [24, 25],

$$D = (1/3)\int_0^\infty C_v(x)\,dx \tag{14}$$

where if v is the velocity of an arbitrary molecule,

$$C_v(t) = \langle v(t)\, v(0)\rangle \tag{15}$$

$$\eta = (V/k_B T)\int_0^\infty C_S(x)\,dx$$

where

$$C_S(t) = \langle P_{xy}(t)\, P_{xy}(0)\rangle \tag{17}$$

where

$$P_{xy} = \left\{\sum_{i=1}^{N} m_i v_{xi} v_{yi} - \sum_{i=1}^{N}\sum_{j=1}^{N} (r_{xij} r_{yij})(d\phi_{ij}/dr)/2\, r_{ij}\right\}/V \tag{18}$$

where v_{xi} is the x component of v and r_{xij} is the x component of r_{ij}.

$$\eta_B = (V/k_B T)\int_0^\infty C_B(x)\,dx \tag{19}$$

$$C_B(t) = \langle (P(t)-\langle P\rangle)\,(P(0)-\langle P\rangle)\rangle \tag{20}$$

$$\lambda = (V/k_B T^2)\int_0^\infty C_T(x)\,dx \tag{21}$$

where

$$C_T(t) = \langle J_x(t)\, J_x(0)\rangle \tag{22}$$

and J_x is the heat flux in the x direction,

$$J_x = (1/2V)\left(\sum_{i=1}^{N}\left\{v_{xi} A_i + v_{xi}\sum_{j=i}^{N}(r_{xij}\, r_{xij})\phi'/r_{ij}\right.\right.$$

$$\left.\left. + v_{yi}\sum_{j=i}^{N}(r_{xij} r_{yij})\phi'/r_{ij}\right.\right.$$

$$+ v_{zi} \sum_{j=i}^{N} (r_{xij} r_{zij}) \phi' / r_{ij} \Big) \tag{23}$$

where $\phi' = d(\phi_{ij})/dr$ at $r = r_{ij}$ and,

$$A_i = m_i v_i^2 + \sum_{j=i}^{N} \phi_{ij} \tag{24}$$

and

$$T = \sum_{i=1}^{N} m_i \mathbf{v}_i^2 / 3k_B \tag{25}$$

Time origins were started every time step. The mean square displacements, $\Delta r^2(t)$, were also used to provide confirmation of D by the velocity ACF route.

$$\Delta \mathbf{r}^2(t) = \left\langle \sum_{i=1}^{N} (\mathbf{r}_i(t) - \mathbf{r}_i(0))^2 \right\rangle / N \tag{26}$$

$$6D = \lim_{t \to \infty} d(\Delta \mathbf{r}^2(t))/dt \tag{27}$$

Simulations were performed at constant total energy. This was preceded by two equilibration periods: (i) at constant kinetic energy or "temperature" using the "Gaussian Isokinetic" scheme and (ii) at constant total energy. These ensembles were generated using a large time step version of the Verlet "Leapfrog" algorithm [26]. Equilibration was for typically half the duration of the production run.

The time step duration, Δt, was typically 0.01 LJ reduced units. The simulations were performed on $N = 108$ and 256 particle systems to assess the finite size effects or N-dependence. The production simulations, during which the transport coefficients were evaluated, were conducted for Ca. 10 and 2×10^5 time steps, respectively.

The computations were performed in single precision on two CRAY-1S's at the University of London Computer Centre.

2.2 Cluster Search

During the simulation, each time step we analysed the Molecular dynamics configurations for clusters. These can extend beyond the real simulation box; image particles having the same "priority" as real cell Molecular dynamics particles. A group of molecules is in a cluster if they are connected together, as defined in the Introduction. In particular, we look for clusters that percolate (again defined in the Introduction). The criterion for this used in the algorithm is that starting from a (real or image) molecule in the cluster one can walk within the replica lattice or Molecular dynamics boxes to another image of that molecule and still remain in the cluster. If so then it follows that one may also continue to traverse the infinite replica system. The FORTRAN algorithm for performing this task is given in the Appendix. For the purposes of this discussion we confine are analysis of these clusters to the quantity P_c the percolation fraction – the fraction of Molecular dynamics configurations that manifest 1 or more percolating clusters. (*A finite N* system can exhibit more than 1 percolating cluster at any time.) We also calculate the cluster number, n_s – the average number of clusters containing s molecules per time step. These quantities have been

discussed previously [13, 27]. We also look at cluster resolutions of the configurational energy and moduli.

3 RESULTS AND DISCUSSION

3.1 Physical Properties

The density dependence of a selection of the thermodynamic and mechanical properties, and transport coefficients is presented in Figures 2–7. The data presented is for $T = 1.456$. The LJ reduced density is converted to that of an "effective" hard sphere fluid by Equations (28) and (29). These relationships attach a hard sphere diameter to the LJ molecule by empirically matching Enskog hard sphere and *LJ* transport coefficients [28].

$$\sigma_{HS}(T)/\sigma_{LJ} = 1.0217\,(1 - 0.0178/T^{1.256})/T^{1/12} \tag{28}$$

$$\varrho_{HS}/\varrho_{LJ} = (\sigma_{HS}(T)/\sigma_{LJ})^3 \tag{29}$$

The hard sphere diameter and number density are σ_{HS} and ϱ_{HS} respectively. (For clarity we refer to the *LJ* diameter and reduced density as σ_{LJ} and ϱ_{LJ} in this context.) To make the simulation data more widely informative, we further reduce the density to a volume or packing fraction, ϕ, using Equation (30).

$$\phi = \pi\,\varrho_{HS}\sigma_{HS}^3/6 \tag{30}$$

The quantity, ϕ, is the volume occupied by the particles, divided by the total volume. It enables the *LJ* properties to be compared with those of other fluids, such as dispersions and powders, because their particulate number density is conventionally quoted in terms of ϕ.

We consider now the thermodynamic state of the system, as represented by the pressure. In Figure 2 we plot logarithmically the *LJ* reduced pressure, P, from Equation (8) against ϕ. Note that being close to the *LJ* critical density ($T = 1.30$ [29])

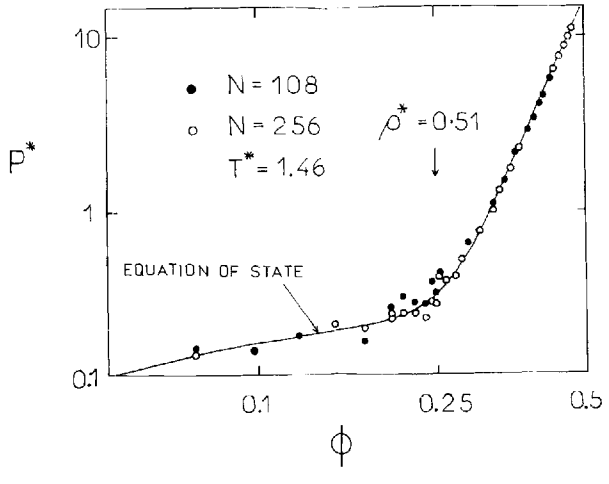

Figure 2 Pressure from Equation (8) versus volume fraction, ϕ.

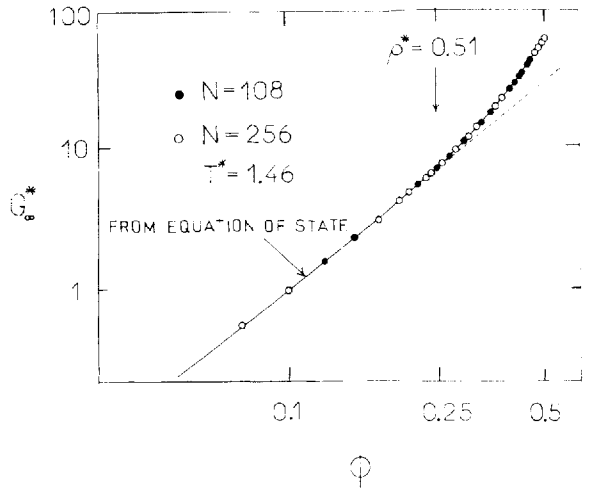

Figure 3 Shear rigidity modulus from Equation (10) versus ϕ. The solid line uses the parameterised equation of state [30] in Equation (12).

there is some statistical uncertainty in the pressure at intermediate densities ($\varrho_{LJ} \approx 0.5$). In low and high density limits the pressure appears to vary as ϕ^n. There is a marked increase in the value of n in the vicinity of $\phi \approx 0.25$. The pressure from a *LJ* equation of state [30] fits the Molecular dynamics data well, but evidently hides the greater pressure fluctuations near $\phi = 0.25$.

We now consider the mechanical properties of the *LJ* fluids. Figure 3 shows the simulation $G_\infty(\phi)$ from Equation (10). They show a much gentler change in slope of the curve at $\phi \approx 0.25$. Interestingly, the simulation G_∞ do not show much scatter in

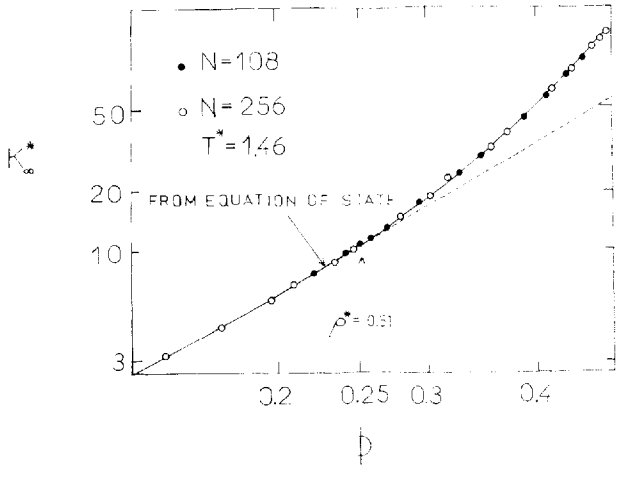

Figure 4 Compressional modulus from Equation (11) versus volume fraction, ϕ. The solid line uses the equation of state [30] in Equation (13).

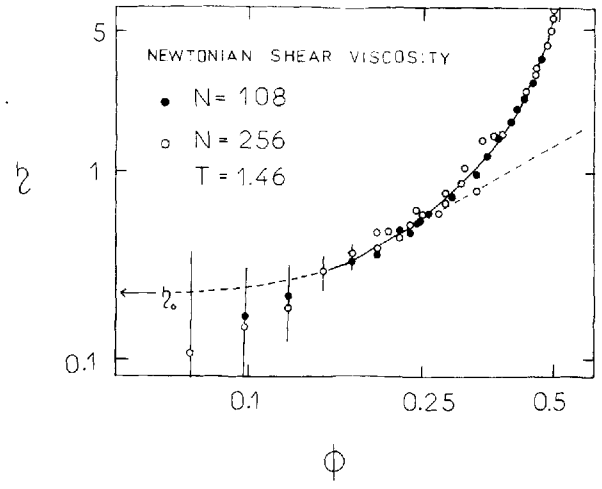

Figure 5 Shear viscosity from Equation (16) versus ϕ.

this regime (in marked contrast to P). The predictions of the *LJ* equation of state, via Equation (12), are also shown on the figure. Excellent agreement between these two independent routes is to be seen. Figure 5 shows the ϕ-dependence of the infinite frequency compressional modulus, K_∞, obtained directly from Equation (11) and predicted from Equations (12) and (13). Its behaviour is qualitatively the same as for $G_\infty(\phi)$, showing an increase in slope at $\phi \approx 0.25 (\varrho^* = 0.51$ at $T^* = 1.46)$.

We now consider the transport coefficients. The data is taken from Table 1 and reference [25]. The shear viscosity is considered in Figure 5. In the limit of zero density (ϕ) the value of η is finite [28] and at this temperature equals 0.22. In this limit the statistical efficiency of Molecular dynamics deteriorates. Nevertheless, taking into

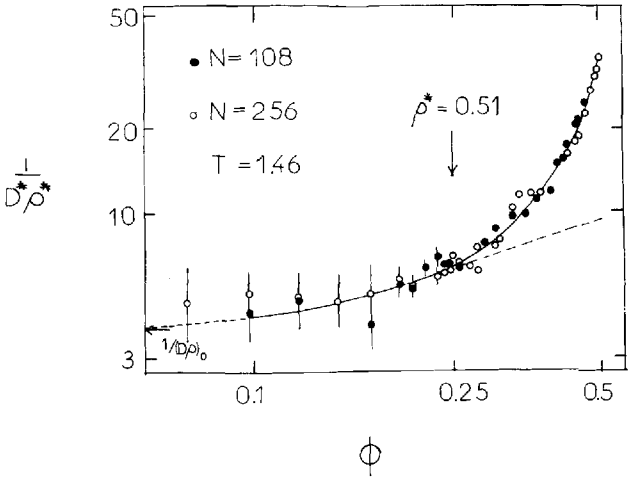

Figure 6 $(D^*\varrho^*)^{-1}$ versus ϕ, where D is evaluated from Equations (14) and (27).

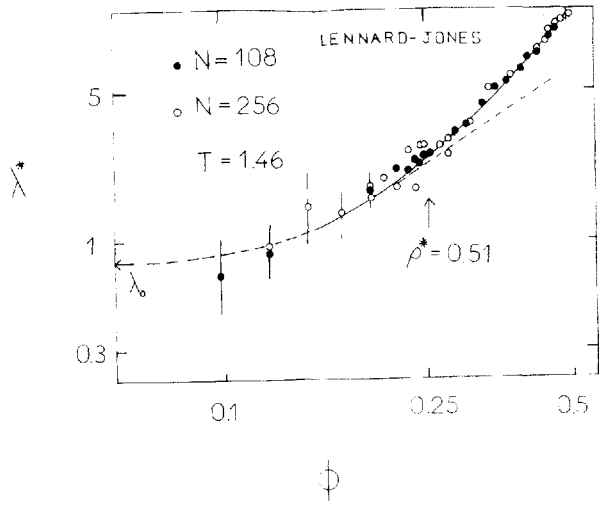

Figure 7 Thermal conductivity from Equation (21) versus ϕ.

account the known asymptotic limit as $\varrho \to 0$, then a clear trend is evident. The steep rise in property with ϕ above $\phi = 0.25$ is even more marked for the shear viscosity than for the previously considered thermodynamic and mechanical properties (certainly exceeding that of the shear modulus). The quantity, $(D^*\varrho^*)^{-1}$ also tends to a density independent limit as $\varrho \to 0$, [3], being equal to 3.7 at $T = 1.456$. Figure 6 shows that the behaviour of $(D^*\varrho^*)^{-1}$ qualitatively follows η over the ϕ range studied, showing a precipitous rise above $\phi = 0.25$. In Figure 7 we present the ϕ dependence of λ, which is seen to be much weaker than for η or $(D\varrho)^{-1}$. Interestingly, the slope of $\lambda(\phi)$ shows only a moderate increase at $\phi = 0.25$. The bulk viscosity, η_B, calculated in Equation (19) and tabulated in Table I are too statistically uncertain to be of use analysed in the above manner. The physical property data up to $T = 10$ were analysed in a similar fashion to reveal that $\phi \approx 0.25$ applies up to $T = 10$. The shear viscosity of the square well fluids [31, 32] also show a similar rise near to $\phi = 0.25$ using the typical value of well-width equal to $\sigma/2$.

3.2 Determination of the Percolation Transition

We postulate that the formation of large clusters of diverging dimensions is the cause of the significant transition in physical properties at $\phi \approx 0.25$. The percolation properties of the *LJ* fluids were investigated primarily to determine at what value of δ the value of ϕ equals 0.25. Using a search diameter, $(1 + \delta)\sigma_{LJ}$, it was discovered that the percolation transition (the value of ϕ where the percolation fraction equals 0.5 for the finite system [17]) is very sensitive to small changes in δ in the vicinity of $\phi_p = 0.25$, as Figure 8 reveals. In this figure we consider $P(\phi)$ for $\delta = 0.11, 0.12$ and 0.13. A comparison between $N = 108$ and 256 states reveals that at a particular δ, for finite N, the percolation packing fraction *decreases* fractionally with increasing N, in the range $N = 108$ and 256. This is consistent with the predictions of finite size effects in Percolation Theory, which predicts that the *Finite-N* ϕ_p should diminish as $\approx N^{-0.38}$ [17]. Using this finite-scaling correction we predict that $\delta = 0.115 \pm 0.002$ gives the

Table 1 Transport coefficients of the Lennard-Jones fluids.

ϱ	D	η	λ	η_B
0.15	(1.39)	(0.11)	(0.30)	(0.05)
0.175	(1.15)	(0.18)	(0.80)	(0.08)
0.20	1.13 (0.96)	0.34 (0.15)	1.37 (0.60)	0.33 (0.12)
0.225	0.75	0.23	0.91	0.08
0.25	0.81 (0.79)	0.22 (0.19)	0.88 (0.94)	0.11 (0.23)
0.35	0.72 (0.56)	0.34 (0.37)	1.37 (1.35)	0.33 (0.20)
0.40	0.45 (0.44)	0.36 (0.40)	1.73 (1.60)	0.36 (0.29)
0.425	0.44 (0.43)	0.47 (0.50)	1.95 (2.00)	0.35 (0.56)
0.45	0.35 (0.35)	0.49 (0.45)	2.19 (1.80)	0.55 (0.50)
0.475	0.31 (0.33)	0.48 (0.53)	2.15 (2.66)	0.27 (0.59)
0.49	0.30 (0.32)	0.54 (0.63)	2.41 (1.76)	0.45 (0.51)
0.50	(0.31)	(0.59)	(2.81)	(0.67)
0.505	0.30 (0.32)	0.58 (0.61)	2.57 (2.59)	0.42 (0.49)
0.51	0.30 (0.28)	0.62 (0.61)	2.52 (2.82)	0.42 (0.55)
0.525	0.25 (0.25)	0.61 (0.64)	2.58 (2.57)	0.62 (0.93)
0.57	(0.29)	(0.68)	(2.55)	(0.38)
0.62	0.18	0.88	3.52	0.51
0.63	(0.19)	(1.06)	(3.55)	(0.50)
0.67	0.15 (0.14)	0.98 (0.80)	4.40 (4.52)	0.53 (0.72)
0.69	(0.12)	(1.49)	(5.18)	(0.73)
0.71	0.14	1.23	5.20	0.63
0.73	(0.12)	(1.56)	(3.90)	(0.91)
0.75	0.12	1.51	5.59	0.68
0.80	0.10	1.86	6.34	0.83
0.825	0.08	2.17	7.25	0.59
0.85	0.075	2.43	7.32	0.28

The reduced density is ϱ, the transport coefficients are defined in the text. The values for D were taken from the msd at low density and the vacf at high density ($\varrho > 0.35$). The numbers refer to $N = 108$ simulations and, in brackets, $N = 256$. $T = 1.456$. The standard errors for D, η and λ are ca. $\pm 10\%$ for $\varrho \lesssim 0.5$ and $\pm 5\%$ for $\varrho \gtrsim 0.5$. These figures are $\pm 35\%$ and $\pm 25\%$, respectively, for η_B.

$(N \to \infty)\, \phi_p = 0.25$ from the data in Figure 1. The sensitivity of ϕ_p to δ around $\delta = 0.12$ at $T = 1.456$ is due to the rapid variation in number of nearest neighbours at the separation $1.12\sigma_{LJ}$ as evidenced in the pair radial distribution function $g(r)$ shown in the insert in Figure 8. This separation occurs just beyond the first peak of $g(r)$, representing the first coordination shell. It also coincides with a point in the pair potential (also shown on Figure 8) where it varies significantly with distance. We note therefore that the importance of $\phi_p \approx 0.25$ arises from the implied physical distance scale, δ, in the fluid, very close to the most probable nearest neighbour distance.

A wider range of δ and temperatures up to 10 were considered. For example at $T = 1.456$ we considered $\delta = 0.05$, 0.15 and 0.2. These give preliminary values for ϕ_p as 0.36, 0.20 and 0.1, respectively. At $T = 10$, for $\delta = 0.0$, 0.05, 0.10 and 0.15 the ϕ_p are *Ca.* 0.22, 0.18, 0.15 and 0.11, respectively. The critical distance scales as the effective-hard sphere diameter. At $T = 1.5$ and 10 then $\sigma_{HS}/\sigma_{LJ} = 0.98$ and 0.84, respectively. The critical distances for percolation are 1.115 and *Ca.* 0.96. These numbers scale with temperature by the same factor (i.e., 1.16). Taking into account the decrease in effective hard-sphere diameter with increasing temperature (from Equation (28)) we conclude that ϕ_p is effectively independent of N, in agreement with the conclusions derived form the physical properties in Section 3.1. Figure 9 shows the percolation transition line corresponding to $\phi_p = 0.25$ for the *LJ* fluid on its (T, ϱ)

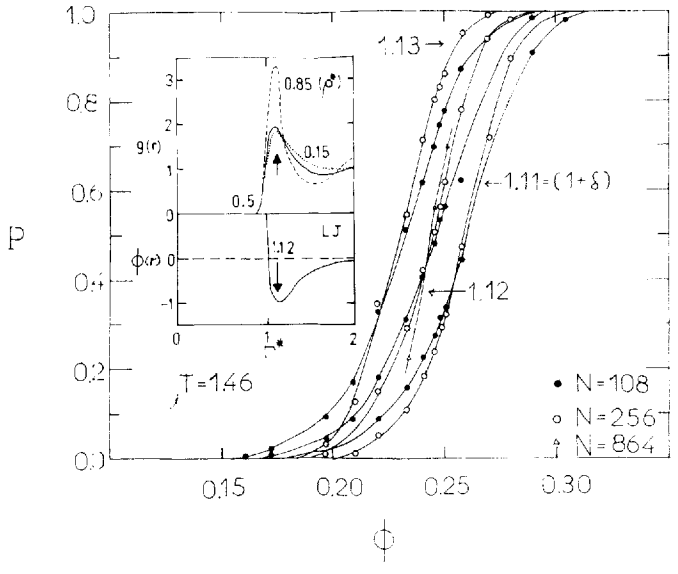

Figure 8 Percolation Probability versus ϕ for three choices of δ. The inserts are the pair radial distribution function $g(r)$ and the Lennard-Jones (LJ) potential from Equation (4).

phase diagram [33, 34]. Due to the inadequacy of Molecular dynamic in representing the critical region, we have not determined the terminus of this line. However, it is possible that it could terminate on the liquid-vapour coexistence line as indicated in the figure. For this we refer to the work of Coniglio *et al.*, who used Hill's concept of bound pairs to predict that for a van der Waals fluid the percolation line should terminate on the liquid-vapour coexistence line at a density *less* than the critical density [35]. It is not clear whether or not the percolation line is a true thermodynamic phase transition (i.e., possessing a singularity in some high order derivative of the free energy with respect to a thermodynamic variable). This question has also been raised in the work of van Swol and Woodcock for free volume percolation [14].

3.3 Analysis of Clusters

We now consider cluster distribution, $n_s(s)$, and a resolution of the physical properties into the contributions from the individual clusters. In Figure 10 we portray $sn_s(s)$, which is the number of atoms to be found in a cluster of size s as a function of s, for three state points spanning $P = 0.5$ for $\delta = 0.12$ and $T = 1.456$. We further resolve our clusters into the percolating components as well as the total analysis. As the percolation transition is crossed there is a transfer of particles from small to large clusters comparable to N. In the transition regime the function $sn_s(s)$ is bimodal. (For random percolation $n_s(s)$ has a simple power law decay in s [13]). At higher density the peak close to N becomes skewed with a tail descending to low cluster number but at high s it is truncated by the limitation that $s \leqslant N$ for these finite periodic systems. The number of nearest neighbours is not a well-defined quantity for continuum systems but if we count all neighbours separated by less than $1.115\sigma_{LJ}$ (to be consistent with our definition of the most physically significant percolation line) then the

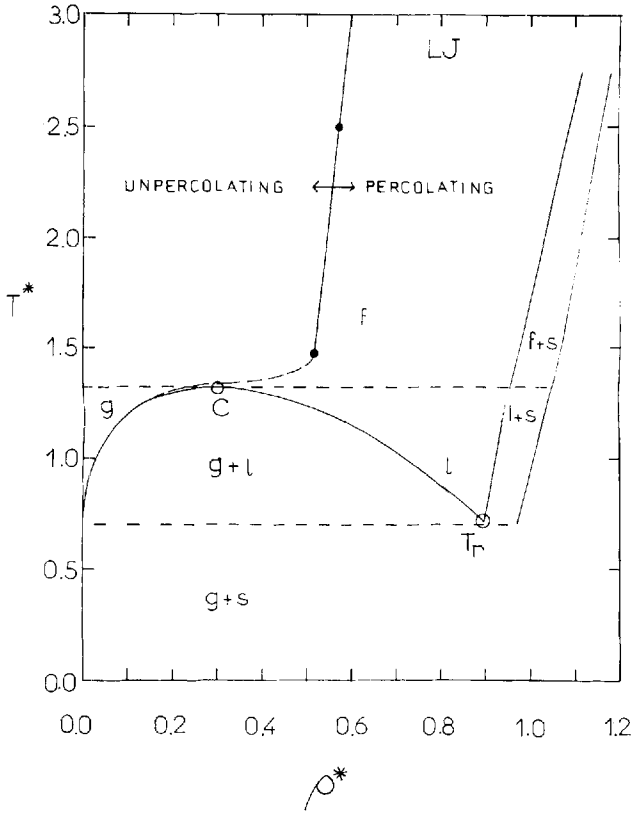

Figure 9 The LJ phase diagram and the percolation line for $\phi_p = 0.25$.

number is 2.0 ± 0.1 at percolation ($T = 1.456$). This value is close to the hard-core limit of 1.5 [16].

In Figure 11 we consider the potential energy per particle, Φ_i, as a function of cluster size. We show the energy derived from within the cluster ("intra") and from all other particles plus long range correction (total or "intra + inter + lrc"). The picture established from $sn_s(s)$ at percolation is of a few large clusters and small clusters filling the voids within the large clusters. Φ_i supports this view. The intra component has a slow monotonic decay towards the total value because of "missing" interactions arising from "void" clusters. Note that for molecules in small clusters (which by definition are more isolated from most of their neighbours than those in the larger clusters) the *total* Φ_i manifests a less negative value than for particles in the large clusters, reflecting their more relative isolation.

The pair potential is used directly to obtain Φ_i. It is a long range probe, unlike its first and second derivative used to obtain the moduli. In Figure 12 we show a cluster resolution of the % contributions to the total G_∞ (using the direct expression in reference [36]) for the same states as for Figure 10. This function largely follows the trends in $sn_s(s)$. The intra/total comparison is very different to that of Φ_i. There is little difference between intra and total because the modulus is a measure of short range interactions contained within the truncation radius ($1.12\sigma_{LJ}$, here). A cluster resolu-

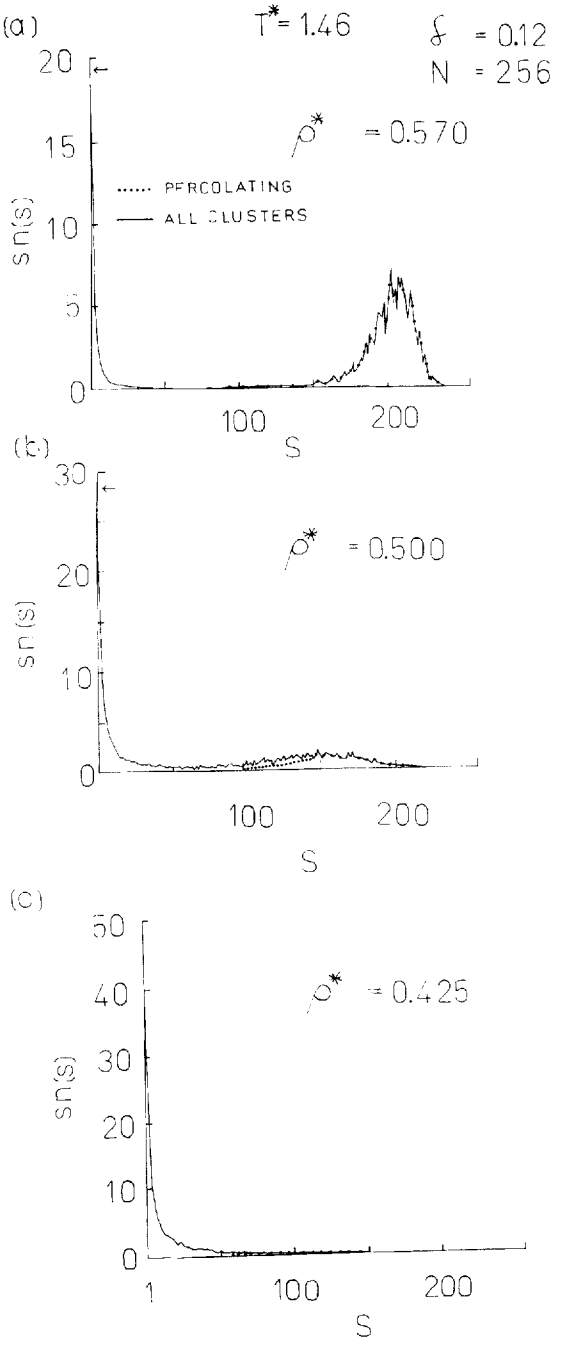

Figure 10 The distribution of molecules in clusters $sn_s(s)$, where s is the number of particles in a cluster. $1 \leqslant s < N$.

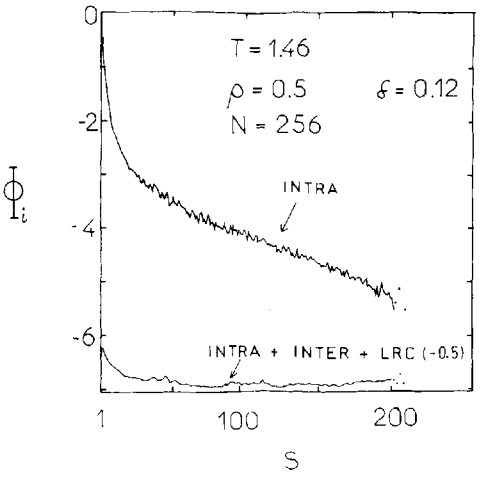

Figure 11 The potential energy per particle, Φ_i, as a function of s. INTRA only takes interactions from within the same cluster. INTER includes interactions from all other clusters. LRC is the long range correction to the energy.

tion of K_∞ follows similar behaviour, although the second peak becomes comparably pronounced at marginally lower densities.

A number of questions remain. To what extent are these changes in physical properties driven by the geometrical changes of the percolation transition? Why should a percolation transition, characterised by a change of the long range structure, influence such properties as the pressure, which are determined mainly by short range interactions within the first coordination shell? An examination of the pair radial distribution function and integrated coordination numbers, CN, reveals that at $\phi_p \approx 0.25$ there is a distinguishable increase in the slope of $CN(\phi)$. For example, using a cut-off of $1.16\sigma_{LJ}CN$ is 1.0, 2.0, 3.3, and 5.5 at ϕ equal to 0.1, 0.2, 0.3 and 0.4. Similar anomalies are seen in the position of the first peak in $g(r)$. Analysing the $T = 1.456$ isotherm, we find the following trend. The position of the first peak in the pair radial distribution function decreases from a value of 1.100 ± 0.005 at densities below the percolation transition, at $\varrho = 0.51$. The descent is linear with density increase, achieving a vlaue of 1.050 ± 0.002 at a density of 0.9.

The formation of large clusters is also, therefore, associated with local structural changes which impinge on physical properties. We suggest that the percolation transition has a strong impact on short range structure. This explains why even the transport coefficients are sensitive to the percolation transition, because they are probes of force fields determined by local structure. It only requires *ca.* 1–2 psec to obtain these from the Green-Kubo relationships, by which time the molecules have only moved *ca.* 1 molecular diameter, reflecting an on-average unchanged local distribution of neighbours.

We observed that the changes in physical properties with ϕ become smoother with increasing temperature. Only close to the critical temperature are there sharp transitions at $\phi_p \approx 0.25$, separating two linear regimes on log-log plots. This is to be expected as with increasing temperature the molecules explore a much wider range of the interaction potential so that there is even less support for a single characteristic

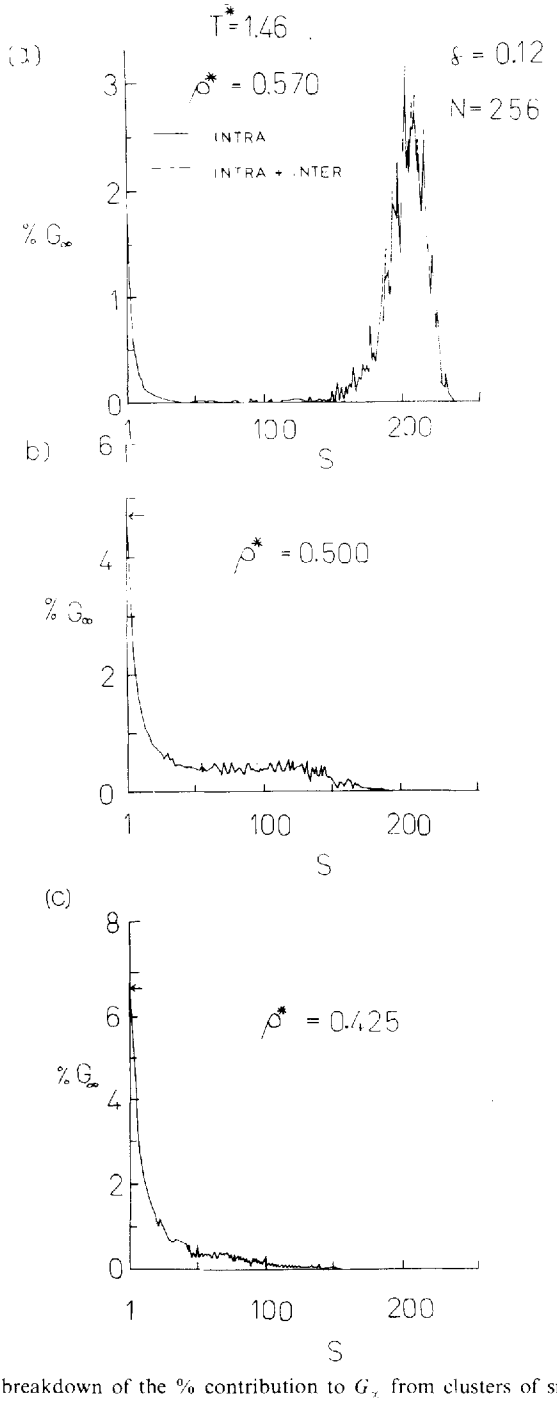

Figure 12 A cluster breakdown of the % contribution to G_∞ from clusters of size s. States cross the percolation transition.

size of the particles – an implicit feature of the theory of random percolation. We must therefore be careful not to associate a high temperature system with classical random percolation, where there is still a well-defined excluded volume to the particles. Only at low temperature is a distinct transition in physical properties associated with the percolation transition, at higher temperature the effect is broadened by a the kinetic smearing of the range of particle sizes.

Preliminary analysis of logarithmic plots of physical properties against $(\phi - \phi_p)$ do not reveal any critical behaviour, as normally obtained in percolation systems [13]. The power law behaviours ϕ^n observed at low temperatures suggest simple mean field treatments incorporating the local structural changes described above may account for physical properties above ϕ_p. The exponents n were found to be temperature dependent.

4 CONCLUSIONS

In this paper we have interpreted the physical properties of a simple fluid in terms of its inherent cluster size distribution. We have shown that there is a noticeable change in the density dependence of thermodynamic, mechanical and transport coefficients at an effective volume fraction of *Ca.* 25%. This point occurs when fluid molecules that "just-touch" are connected through all space (they are said to percolate). This infinitely spanning cluster confers a connectivity-related departure on the physical properties. We have not established the temporal nature of these clusters.

Acknowledgements

D.M.H. gratefully thanks *The Royal Society* for the award of a *Royal Society* 1983 *University Research Fellowship*. J.R.M. thanks the S.E.R.C. for financial support. The University of London Computer Centre is thanked for a generous allocation of computer time. We would also like to thank Dr. D. Brown (U.M.I.S.T.) for bringing ref. [37] to our attention.

Appendix

In this appendix the Fortran code for searching for clusters and identifying percolation is described. The code is written below as a self-contained subroutine. Periodic boundary conditions are applied in the calculation of interparticle distances. The algorithm obeys the following specifications.

(i) Given coordinate arrays *RX*, *RY*, *RZ* for NOM particles in a cubic box of side BOXL and separation parameter SEP, the routine partitions the set of particles into disjoint subsets – the clusters, such that for all particles in a cluster all other particles lying within a distance SEP of the particle, or with a periodic image lying within SEP, are also in the same cluster.

(ii) Each cluster found is tested for percolation in the infinite replica system. (see text and Seaton and Glandt [17]).

The algorithm finds clusters iteratively, searching for all neighbours within SEP of the present site. Then it searches around the neighbours so found for their neighbours within a distance SEP and so continuing iteratively. As the algorithm proceeds the

present cluster being found is stored in an array ICLUS. The elements ICLUS(1) to ICLUS(k1 − 1) contain the indices of those particles in the present cluster for which the algorithm has already found neighbours within SEP. ICLUS(ki) contains the index of the particle for which the algorithm is presently searching for neighbours (within SEP). ICLUS(k1 + 1) to ICLUS(k2) contains the indices of those particles already found to be in the cluster but for which the algorithm has not yet searched for neighbours within SEP. A cluster is completed when all neighbours of the present site have already been found to be in the cluster and k1 = k2.

To discover if a particular cluster is percolating the algorithm keeps track of which replica of a particle has been found as a neighbour. It is easy to prove that if and only if the cluster is percolating then during the cluster search some particle, already found to be in the cluster, will be found as a "neighbour," but as a different replica from that found previously. This simple test for percolation adds little time to the basic search algorithm.

The central loop of the code, loop 60, may be written in a vectorised form for a vector processor, such as, the CRAY-1S used in the present work. A more efficient cluster searching algorithm is given by Bunz [37], however this code is incompatible with the above percolation test.


```
      PARAMETER (NOM=108,BOXL=1.0)
      SUBROUTINE CLUSTER(SEP,N)
      LOGICAL FLGPERC
      COMMON/COOR/ RX(NOM),RY(NOM),RZ(NOM)
      DIMENSION GOT(NOM),ICLUS(NOM),CELLX(NOM),CELLY(NOM),CELLZ(NOM)
     X,IORNE(NOM),TCELLX(NOM),TCELLY(NOM),TCELLZ(NOM)
      DO 10 I=1,N
10    GOT(I)=0.0
      SEP2=SEP*SEP
      DO 20 IS=1,N
C     START A SEARCH FOR A NEW CLUSTER.
C     CHECK IF THE MOLECULE THE HAS ALREADY BEEN INCLUDED IN A CLUSTER
      IF (GOT(IS).EQ.1.0) GOTO 20
      GOT(IS)=1.0
C     ICLUS HOLDS THE INDICES OF THE MOLECULES IN THE GROWING CLUSTER
C     CELLX,CELLY,CELLZ CONTAIN THE VECTORS DENOTING WHICH IMAGE OF
C     A MOLECULE HAS BEEN FOUND TO BE IN THE CLUSTER.
      DO 30 I=1,N
      ICLUS(I)=0
      CELLX(I)=0.0
      CELLY(I)=0.0
      CELLZ(I)=0.0
30    CONTINUE
      ICLUS(1)=IS
      FLGPERC=.FALSE.
      K1=0
      K2=1
50    K1=K1+1
C     K1 IS THE CLUSTER PARTICLE OF IMMEDIATE INTEREST.
C     K2 IS THE INDEX OF THE LAST CLUSTER PARTICLE.
      IO=ICLUS(K1)
C     NOTE WHICH MD CELL "IO" IS IN.
      IOX=INT(CELLX(IO))
      IOY=INT(CELLY(IO))
      IOZ=INT(CELLZ(IO))
      OX=RX(IO)
      OY=RY(IO)
      OZ=RZ(IO)
C     LOOK FOR THE NEIGHBOURS OF "IO".
C     SEP2 IS THE SQUARE OF THE SEARCH DIAMETER, (1+DELTA)*SIGLJ.
      M=0
      DO 60 J=1,N
      IF (J.EQ.IO) GOTO 60
```

```
C       LOOP OVER POSSIBLE CLOSE NEIGHBOURS, J, OF "IO".
        DISX=INT(2.0*(OX-RX(J))/BOXL)
        DISY=INT(2.0*(OY-RY(J))/BOXL)
        DISZ=INT(2.0*(OZ-RZ(J))/BOXL)
        XS=OX-RX(J)-DISX*BOXL
        YS=OY-RY(J)-DISY*BOXL
        ZS=OZ-RZ(J)-DISZ*BOXL
        RR=XS*XS+YS*YS+ZS*ZS
        IF (RR.GT.SEP2) GOTO 60
        M=M+1
        IORNE(M)=J
        TCELLX(M)=DISX+FLOAT(IOX)
        TCELLY(M)=DISY+FLOAT(IOY)
        TCELLZ(M)=DISZ+FLOAT(IOZ)
60      CONTINUE
C       ANALYSE THE NEIGHBOURS OF "IO"
        NEWNN=0
        DO 70 J1=1,M
        J=IORNE(J1)
C       IS A NEWLY FOUND NEIGHBOUR, J, ALREADY IN THE CLUSTER?
        IF (GOT(J).EQ.0.0) THEN
C       NO, THEREFORE WE HAVE FOUND A NEW NEIGHBOUR.
        NEWNN=NEWNN+1
C       STORE ANOTHER PARTICLE IN THE LIST TO BE LOCKED AROUND.
        K2=K2+1
        ICLUS(K2)=J
        GOT(J)=1.0
        CELLX(J)=TCELLX(J1)
        CELLY(J)=TCELLY(J1)
        CELLZ(J)=TCELLZ(J1)
        ELSE
C       YES, IF SO, IS IT THE "SAME" J, I.E., NOT ANOTHER "J" SUCH AS AN IMAGE.
        T1=TCELLX(J1)-CELLX(J)
        T2=TCELLY(J1)-CELLY(J)
        T3=TCELLZ(J1)-CELLZ(J)
        T=T1*T1+T2*T2+T3*T3
C       SET FLGPERC IF WE HAVE FOUND A DIFFERENT IMAGE
        IF (T.NE.0.0) FLGPERC=.TRUE.
        ENDIF
70      CONTINUE
        IF ((NEWNN.GT.0).OR.(K2.GT.K1)) GOTO 50
C       WE HAVE JUST COMPLETED ANOTHER CLUSTER, OF K2 PARTICLES
C       IT CAN BE ANALYSED NOW BEFORE GOING TO THE TOP OF THE LOOP
C       AGAIN TO FORM A NEW CLUSTER. FLGPERC INDICATES IF IT PERCOLATES.
20      CONTINUE
        RETURN
        END
```


References

[1] W.T. Ashurst and W.G. Hoover, "Dense-fluid shear viscosity via nonequilibrium molecular dynamics," *Phys. Rev. A.*, **11**, 658 (1975).

[2] D.M. Heyes, "Shear thinning and thickening of the Lennard-Jones liquid: A molecular dynamics study," *J. Chem. Soc. Faraday Trans. II*, **82**, 1365 (1986).

[3] D.M. Heyes and R. Szczepanski, "The rheology of gases: A molecular dynamics study," *J. Chem. Soc. Faraday Trans. II*, **83**, 319 (1987).

[4] D.M. Heyes, "Rheology of molecular liquids and concentrated suspensions by microscopic dynamical simulations," *J. Non-Newt. Fluid Mech.*, **27**, 47 (1988).

[5] W. Hirst and A.J. Moore, "Elastohydrodynamic lubrication at high pressures II. Non-Newtonian behaviour," *Proc. R. Soc. London, A*, **365**, 537 (1979).

[6] C.G. de Kruif, E.M.F. van Lersel, A. Vrij and W.B. Russel, "Hard sphere colloidal dispersions: viscosity as a function of shear rate and volume fraction," *J. Chem. Phys.*, **83**, 4717 (1985).

[7] L.V. Woodcock, "Origins of shear dilatency and shear thickening phenomena," *Chem. Phys. Lett.*, **111**, 455 (1984).

[8] D.M. Binding, K. Walters, J. Dheur and M.J. Crochet, "Interfacial effects in the flow of viscous and elasticoviscous liquids," *Phil. Trans. R. Soc. Lond. A*, **323**, 449 (1987).

[9] A.A. Clifford and N. Platts, "Transport properties in dilute gases: An approach using time correlation functions," *J. Chem. Soc. Faraday Trans. II*, **76,** 747 (1980).
[10] R.F. Berg, M.R. Moldover, and J.S. Huang, "Quantitative characterization of the viscosity of a microemulsion," *J. Chem. Phys.*, **87,** 3687 (1987).
[11] E.A. Morriss, A.N. Cutler, S.B. Ross-Murphy, D.A. Rees and J. Price, "Concentration and shear rate dependence of the viscosity in random coil polysaccharide solutions," *Carbohydrate Polym.*, **1,** 5 (1981).
[12] J.T. Chayes and L. Chayes, "Percolation and randommedia," in *Les Hoches, Session XLIII, 1984. Critical Phenomena, Random Systems, Gauge Theories*, eds. K. Osterwalder and R. Stora, Elsevier Science Publishers B.V., 1986.
[13] D. Stauffer, "Percolation and cluster size distribution," in *On Growth and Form*, H.E. Stanley and N. Ostwesky, Martinus Nijhoff, 1986, p. 79.
[14] F. van Swol and L.V. Woodcock, "Percolation transition in the parallel hard-cube model fluid," *Mol. Sim.*, **1,** 95 (1987)
[15] A.L.R. Bug, S.A. Safran, G.S. Grest and I. Webman, "Do interactions raise or lower a percolation threshold?," *Phys. Rev. Lett.*, **55,** 1896 (1985).
[16] I. Balberg and N. Binenbaum, "Invariant properties of the percolation thresholds in the soft-core – hard-core transition," *Phys. Rev. A*, **35,** 5174 (1987).
[17] N.A. Seaton and E.D. Glandt, "Aggregation and percolation in a system of adhesive spheres," *J. Chem. Phys.*, **86,** 4668 (1987).
[18] N.A. Seaton and E.D. Glandt, "Conductivity from simulations of percolating systems of interacting particles," *J. Phys. A*, **20,** 3029 (1987).
[19] I. Webman, "The elastic behavior of fractal structures," in *Fractals in Physics*, L. Pietronero and E. Tosatti, eds, Elsevier, 1986.
[20] E. Guyon, "On the rheology of random matter," p. 163 in *On Growth and Form*, H.E. Stanley and N. Ostwesky, Martinus Nijhoff, 1986.
[21] D.M. Heyes, "Self-diffusion and shear viscosity of simple fluids: a molecular-dynamics study," *J. Chem. Soc. Faraday Trans. II*, **79,** 1741 (1983).
[22] D.M. Heyes, "Thermal conductivity and bulk viscosity of simple fluids: a molecular-dynamics study," *J. Chem. Soc. Faraday Trans. II*, **80,** 1363 (1984).
[23] R. Zwanzig and R.D. Mountain, "High-frequency elastic moduli of simple fluids," *J. Chem. Phys.*, **43,** 4464 (1965).
[24] D.M. Heyes, "Transport coefficients of the Lennard-Jones fluid by molecular dynamics," *Canad. J. Phys.*, **64,** 773, (1985).
[25] D.M. Heyes, "Transport coefficients of Lennard-Jones fluids: A molecular Dynamics and effective hard-sphere treatment" *Phys. Rev. B*, **37,** 5677 (1988).
[26] D. MacGowan and D.M. Heyes, "Large timesteps in molecular dynamics simulations", *Mol. Sim.* **1,** 277 (1988).
[27] H.J. Herrmann, "Geometrical cluster growth models and kinetic gelation," *Phys. Rep.*, **136** 153 (1986).
[28] K.D. Hammonds and D.M. Heyes, "Transport coefficients of model simple liquids: a molecular dynamics study and effective hard sphere analysis," *J. Chem. Soc. Faraday Trans. II*, **84,** 705 (1988).
[29] D.J. Adams, "Calculating the high-temperature vapour line by Monte Carlo," *Molec. Phys.*, **37,** 211 (1979).
[30] J.J. Nicolas, K.E. Gubbins, W.B. Streett and D.J. Tildesley, "Equation of state for the Lennard-Jones fluid," *Molec. Phys.*, **37,** 1429 (1979).
[31] J.P.J. Michels and N.J. Trappeniers, "Molecular dynamical calculations of the transport properties of a square-well fluid. I The viscosity below critical density," *Physica A*, **101,** 156 (1980).
[32] J.P.J. Michels and N.J. Trappeniers, "Molecular dynamical calculations of the transport properties of a square-well fluid. IV The influence of the well-width on the viscosity and the thermal conductivity," *Physica A*, **107,** 299 (1981).
[33] J.-P Hansen and L. Verlet, "Phase transitions of the Lennard-Jones system," *Phys. Rev.*, **184,** 151 (1969).
[34] J.-P. Hansen, "Phase transition of the Lennard-Jones system. II. High temperature limit," *Phys. Rev. A*, **2,** 221 (1970).
[35] A. Coniglio, U. De Angelis and A. Forlani, "Pair connectedness and cluster size," *J. Phys. A*, **10,** 1123 (1977).
[36] D.M. Heyes, "Shear thinning of the Lennard-Jones fluid by molecular-dynamics," *Physica A*, **133,** 473 (1985).
[37] H. Bunz, "Identification of Clusters in computer experiments with periodic boundary conditions," *Comp. Phys. Comm.* **42,** 435 (1986).